Synthesis and electrical characterisation of zinc-doped yttrium oxide

G. Bhavani, S. Ganesan, S. Selvasekarapandian, S. Monisha & M. Premalatha

Ionics
International Journal of Ionics The Science and Technology of Ionic Motion

ISSN 0947-7047

Ionics
DOI 10.1007/s11581-015-1565-1

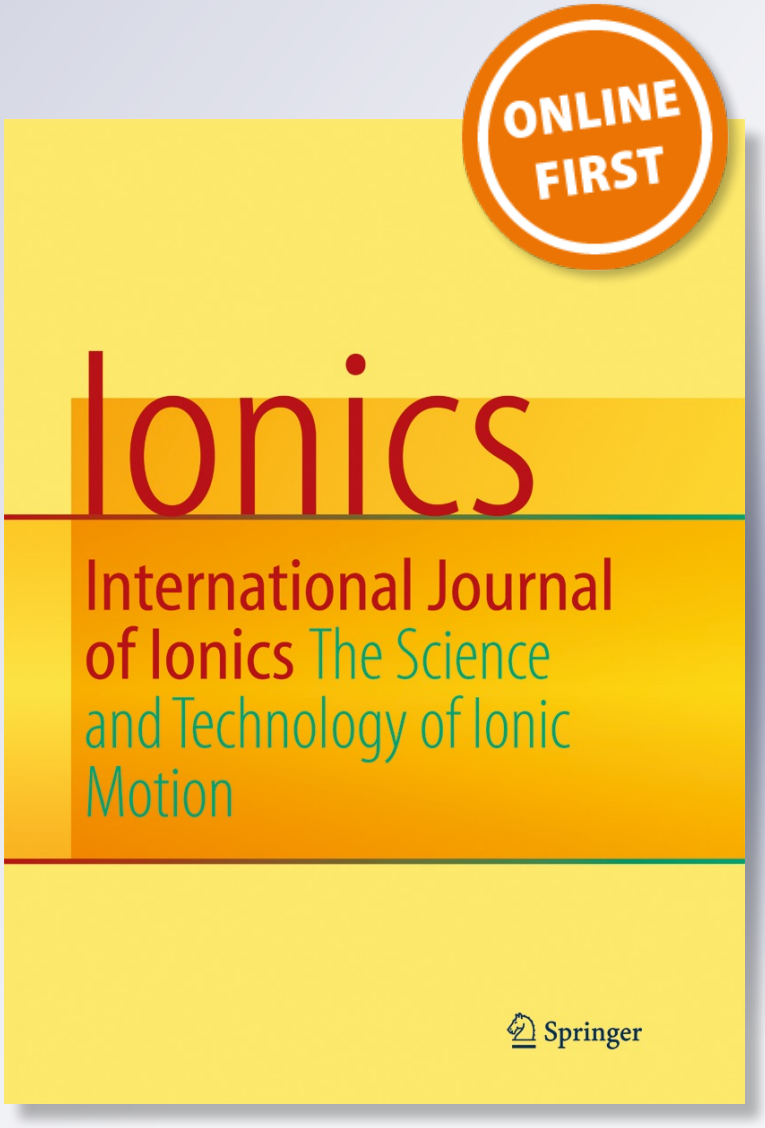

Springer

Ionics
DOI 10.1007/s11581-015-1565-1

ORIGINAL PAPER

Synthesis and electrical characterisation of zinc-doped yttrium oxide

G. Bhavani[1] · S. Ganesan[2] · S. Selvasekarapandian[3] · S. Monisha[3] · M. Premalatha[3]

Received: 25 July 2015 / Revised: 3 September 2015 / Accepted: 20 September 2015

Abstract Zinc-doped yttrium oxide nanopowders of various doping concentrations have been successfully synthesized by simple methods like sol–gel, solvothermal and wetchemical methods. Structural property is analysed by X-ray powder diffraction (XRD). The presence of elements is confirmed by FTIR studies. Conductivity and dielectric behaviour of the samples are analysed by impedance spectroscopy. The effects of doping concentration and method of preparation on the crystallinity, the dielectric constant and the electrical properties of zinc-doped Y_2O_3 nanomaterials are investigated and presented in this paper. XRD analysis shows the crystalline nature of the samples except the one prepared by solvothermal method. Also, the same sample is found to have more conductivity in the order of 5.04×10^{-7} Scm^{-1} when compared with the samples prepared by other methods and of different doping concentration.

Keywords Yttrium oxide · Sol-gel · Solvothermal · Wet chemical · Conductivity · Dielectric · Bulk resistance

Introduction

Nanomaterials with large volume-to-surface area and high dielectric constant are in the focus of current interest not only for purely academic reasons but also for the further development of modern electronics. This is due to the grain barrier effects which occur at nanosize which play an important role on the dielectric properties of the materials, and they exhibit novel catalytic, optical, magnetic and electrical properties relative to those of the bulk materials [1–5]. The regular improvement in display market is extending its study on the next-generation display devices such as organic light-emitting diode (OLED) or flexible display [6, 7].

Y_2O_3 possesses some unique properties. It has a higher melting temperature (2430 °C) than a number of other well-known oxides [8]. Y_2O_3 has a wide energy band gap, high values of electrical resistivity (10^{11}–10^{12} ohm/m), dielectric permittivity (11–15) and electric strength (10^8–10^9 Vm^{-1}), and it also shows low dielectric losses (0.01–0.03) and good transparency in a wide spectral range with little light diffusion [9–13]. Due to these properties, Y_2O_3 is a prospective material for antireflecting and protective coatings, interference mirrors and for manufacturing passive components and dielectric layers in multilevel integrated circuits [10]. Much attention, therefore, has been paid to Y_2O_3 nanomaterials also for memory devices owing to their electrical characteristics and potential applications [14].

AC conductivity of nanomaterials is found to depend on the number of grains and grain boundaries. In order to understand it, the nanostructure-dependent ac conductivity is very important so as to tune the conditions to produce Y_2O_3 nanomaterials for the desired electronic device applications. Hence, fundamental understanding of the electrical properties is important for employing Y_2O_3 nanomaterials in storage capacitors for dynamic random access memories [15–19]. Furthermore, the ability to tailor the properties so as to optimize performance requires a detailed understanding of the relationship between electronic and geometric structure, particularly at the nanoscale dimensions. Frequency-dependent

✉ G. Bhavani
bhavaneeg@gmail.com

[1] Department of Physics, Jansons Institute of Technology, Coimbatore, Tamilnadu, India

[2] Srisakthi Institute of Engineering and Technology, Coimbatore, Tamilnadu, India

[3] Materials Research Center, Coimbatore, Tamilnadu, India

Published online: 03 October 2015

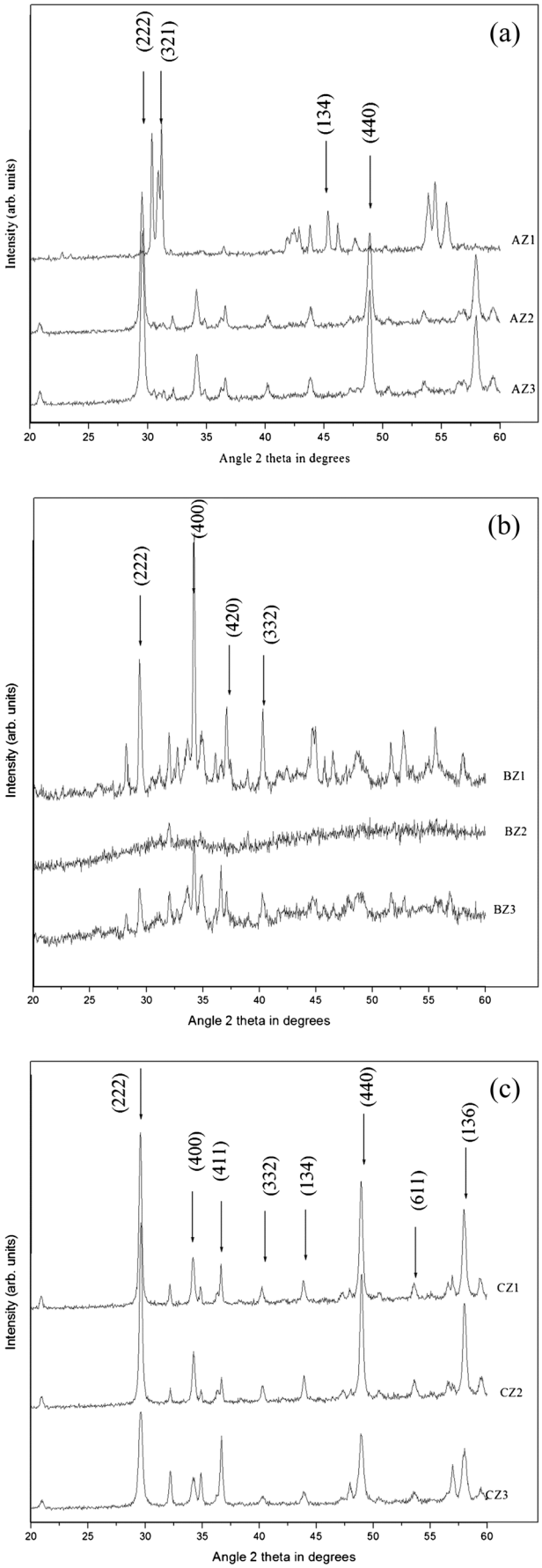

Fig. 1 **a** XRD diffraction patterns of samples AZ1, AZ2, AZ3. **b** XRD ▶ diffraction patterns of samples BZ1, BZ2 and BZ3. **c** XRD diffraction patterns of samples CZ1, CZ2 and CZ3

conductivity, which is a major part of this work apart from structural characterization, is an important analytical method to study the electrical properties, conduction mechanism and the dispersion of relaxation times of Y_2O_3 nanomaterials. Interestingly, we found that there exists a correlation between the microstructure and electrical properties, specifically the grain-size-dependent electrical conductivity.

Optical and structural property of zinc–yttrium system samples is well studied [20]. However, an electrical property of zinc-doped yttrium oxide samples is hardly reported in the literature. In this paper, for the first time, we report the structural and the electrical properties of zinc-doped Y_2O_3 nanomaterials prepared by simple precipitation techniques like sol–gel, solvothermal and wet chemical methods. The effects of doping concentration and method of preparation on the crystallinity, the dielectric constant and the electrical properties of zinc-doped Y_2O_3 nanomaterials are investigated in order to evaluate the feasibility of using Y_2O_3 in OLED, FED, etc.

Experimental

The samples AZ1: Y_2O_3:Zn (1 g of Y : 0.25 g of Zn), AZ2: Y_2O_3:Zn (1 g of Y : 0.5 g of Zn) and AZ3: Y_2O_3:Zn (1 g of Y : 1 g of Zn) are prepared by sol–gel method and BZ1: Y_2O_3:Zn (0.6 g of Y : 0.15 g of Zn), and BZ2: Y_2O_3:Zn (0.6 g of Y : 0.3 g of Zn) and BZ3: Y_2O_3:Zn (0.6 g of Y : 0.6 g of Zn) are prepared by solvothermal method and are previously discussed in our paper [21]. CZ1: Y_2O_3:Zn (1 g of Y : 0.25 g of Zn), CZ2: Y_2O_3:Zn(1 g of Y : 0.5 g of Zn) and CZ3: Y_2O_3:Zn(1 g of Y : 1 g of Zn) are prepared by wet chemical method as described below. The preparation of yttrium–zinc precursor was achieved [22–25] which involves a precipitation reaction between the yttrium nitrate and zinc acetate dihydrate and oxalic acid as precipitant agent. Precipitation was conducted at 80 °C, pH=2 and with a molar ratio between yttrium nitrate and oxalic acid of 2:3. Yttrium nitrate solution (0.3 M) was added together with oxalic acid (0.45 M) into diluted solution of P.R. (1:10). Yttrium–zinc ratio was varied as 25, 50 and 100 weight percentage of yttrium nitrate to get CZ1, CZ2 and CZ3 samples. The precursor post-precipitation stage consists of washing and drying [26]. Ammonium hydroxide, sodium hydroxide and oxalic acid have been used as a solvent in sol–gel, solvothermal and wet chemical method, respectively. Solvothermal method takes a long time to prepare the sample, when compared with other two methods, but it is observed that it gives very good samples. The powder XRD study is carried out using a Shimadzu XRD

Table 1 Details of composition and calculated crystallite size of samples

Sample	Method	Precipitating reagent	Composition	Crystallite Size(nm)	Structure
AZ1	Sol–gel	Ammonium Hydroxide	Y_2O_3:Zn(25 Weight % of Y)	14.7	Cubic
AZ2	Sol–gel	Ammonium Hydroxide	Y_2O_3:Zn (50 Weight % of Y)	29.3	Cubic
AZ3	Sol–gel	Ammonium Hydroxide	Y_2O_3:Zn (100 Weight % of Y)	19.3	Cubic
BZ1	Sol–gel	Sodium Hydroxide	Y_2O_3:Zn (25 Weight % of Y)	29.6	Cubic
BZ3	Solvothermal	Sodium Hydroxide	Y_2O_3:Zn (100 Weight % of Y)	29.66	Cubic
CZ1	Solvothermal	Oxalic acid	Y_2O_3:Zn (25 Weight % of Y)	3.03	Cubic
CZ2	Solvothermal	Oxalic acid	Y_2O_3:Zn (50 Weight % of Y)	3.00	Cubic
CZ3	Wet Chemical	Oxalic acid	Y_2O_3:Zn (100 Weight % of Y)	3.02	Cubic

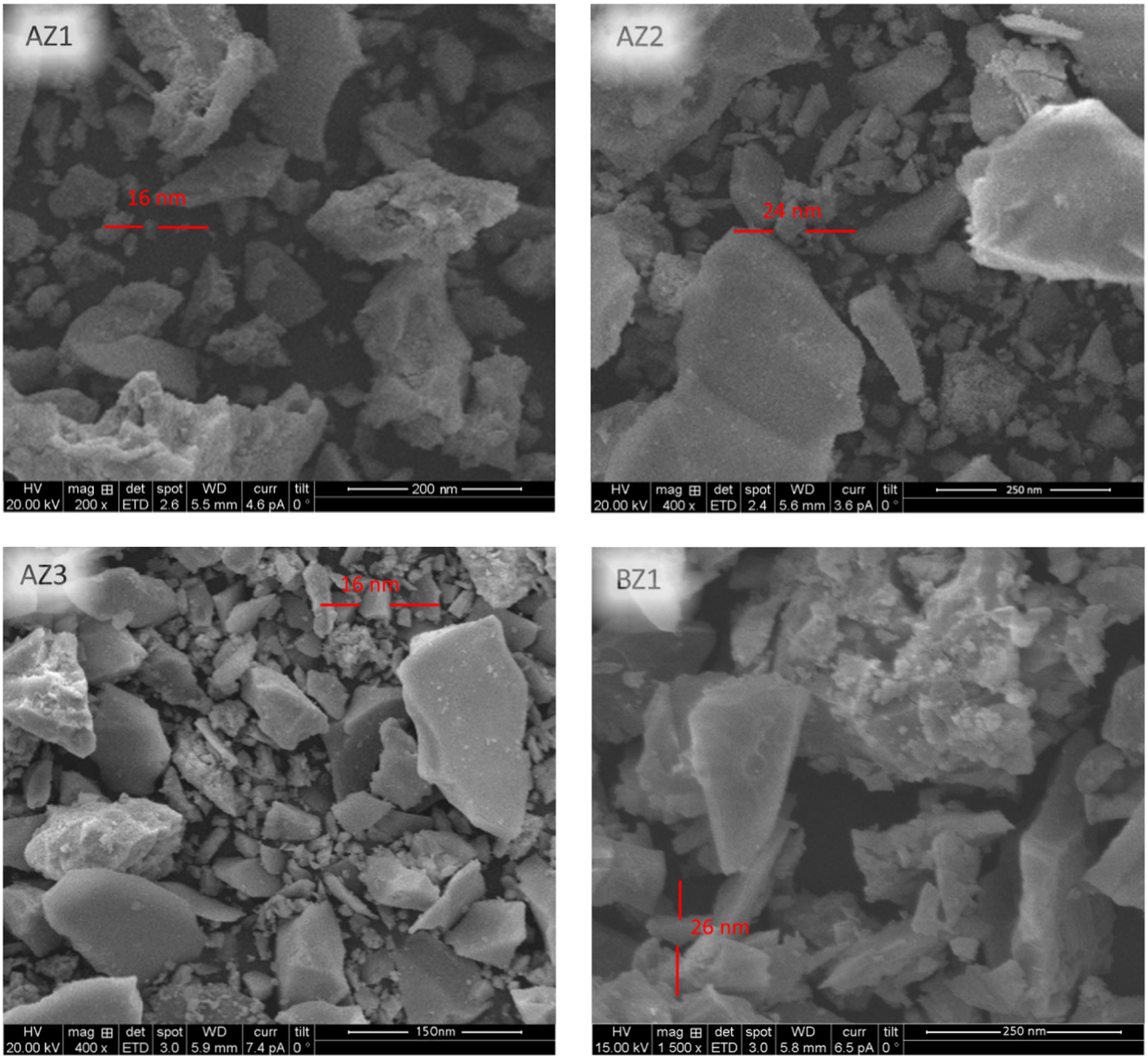

Fig. 2 SEM images of the samples AZ1, AZ2, AZ3 (sol–gel method); BZ1, BZ2 and BZ3(solvothermal method); and CZ1, CZ2 and CZ3 (wet chemical method)

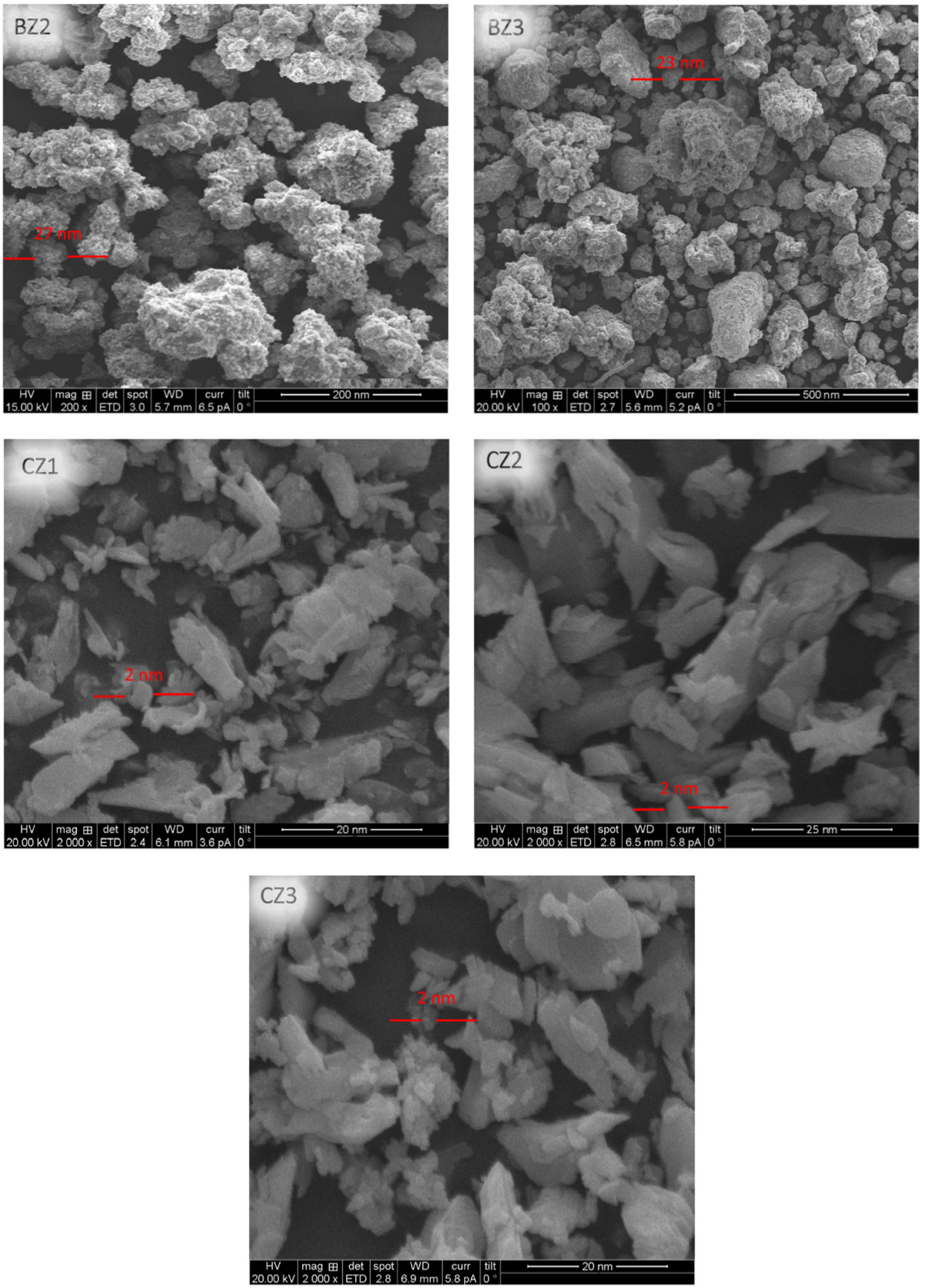

Fig. 2 (continued)

6000 X-ray diffractometer using CuKα radiation. Jasco-FTIR 4100 /japan make is used to take FTIR studies in the range of 500–4000 cm^{-1}. Impedance analysis is done by HIOKI 3532 LCR impedance analyser interfaced with a computer in the frequency range of 42 Hz to 1 MHz at room temperature. The morphological and elemental analysis of the present samples was recorded using SEM coupled with EDAX EOL Model JED – 2300.

Characterisation

XRD

Figure 1a–c shows the XRD patterns of the zinc-doped Y_2O_3 samples prepared using sol–gel, solvothermal and wet chemical methods. The diffractograms all show a small broad peak at ~29° which corresponds to reflections from the <222> planes of Y_2O_3 [27]. The cubic phase of Y_2O_3 is expressed primarily by reflections from the <222> planes [28, 29]. The samples prepared by sol–gel method (AZ1, AZ2 and AZ3) shows the cubic nature of the yttrium oxide and are maintained except with shift in the peak position due to the presence of yttrium hydroxide (JCPDS 832042) formed in the process [21]. Table 1 lists the crystallite sizes of synthesized particles estimated from the well-defined known Debye–Scherrer's equation [30] along with the composition and structure. The samples are preferably orientated along different planes, and the "d" value is compared with standard JCPDS data card (895591) which confirms the cubic structure of the samples. The sample BZ2 prepared by solvothermal method leads to amorphous nature. The peaks at (222), (400), (420) and (322) attributed to cubic structure of yttrium oxide has been suppressed completely by 50 wt% of zinc. The crystal structure has been destroyed and become amorphous in nature.

SEM

SEM diagrams for all the samples are given in Fig. 2, and the particle sizes of the samples observed from SEM are tabulated in the Table 2.

EDAX

From EDAX measurements, weight percentage of the zinc entered in the yttrium oxide lattice has been calculated and it is shown in the Fig. 3. From the figure, it is observed that the weight percentage of zinc varies between 14 and 23 for the samples prepared by sol–gel method and for the samples prepared by solvothermal method it varies between 6 and 10 and for wet chemical method the range is between 3 and 11.

Table 2 The particle sizes of the samples observed from SEM

Sample	Crystallite size(nm) from SEM
AZ1	16
AZ2	24
AZ3	16
BZ1	26
BZ2	27
BZ3	23
CZ1	2
CZ2	2
CZ3	2

FTIR

Figure 4 shows FTIR spectra of pure and zinc-doped yttrium oxide samples prepared by sol–gel, solvothermal and wetchemical methods. Infrared studies were carried out in order to ascertain the purity and nature of the metal nanoparticles. Metal oxides generally give absorption bands in fingerprint region, i.e. below 1000 cm^{-1}, arising from inter-atomic vibrations. The high intensity band centered around 500–600 cm^{-1} is attributed to Y–O stretching mode of Y_2O_3 structure [31]. The absorption band of O_H stretching vibrations that appears around 3400–3500 and 1600 cm^{-1} are of absorbed water. The band around 750–1020 cm^{-1} corresponds to Zn–O stretching and deformation vibration, respectively. The metal–oxygen frequencies observed for the respective metal oxides are in accordance with literature values [32, 33]. V. Parthasarathi and G. Thilagavathi [34] reported similar

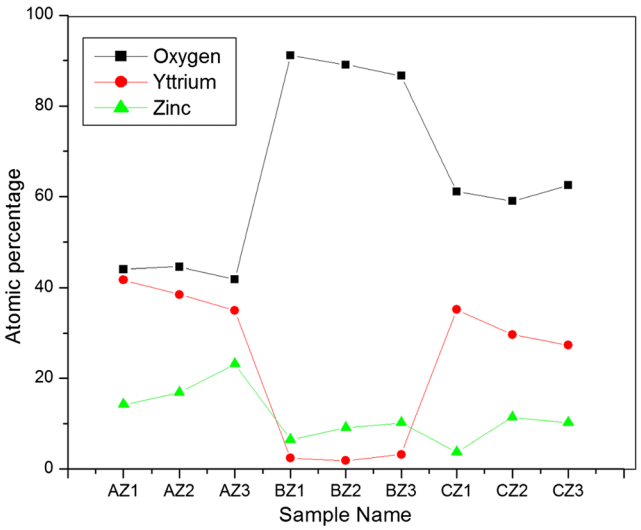

Fig. 3 Comparison of atomic weight percentage of the samples by EDAX studies

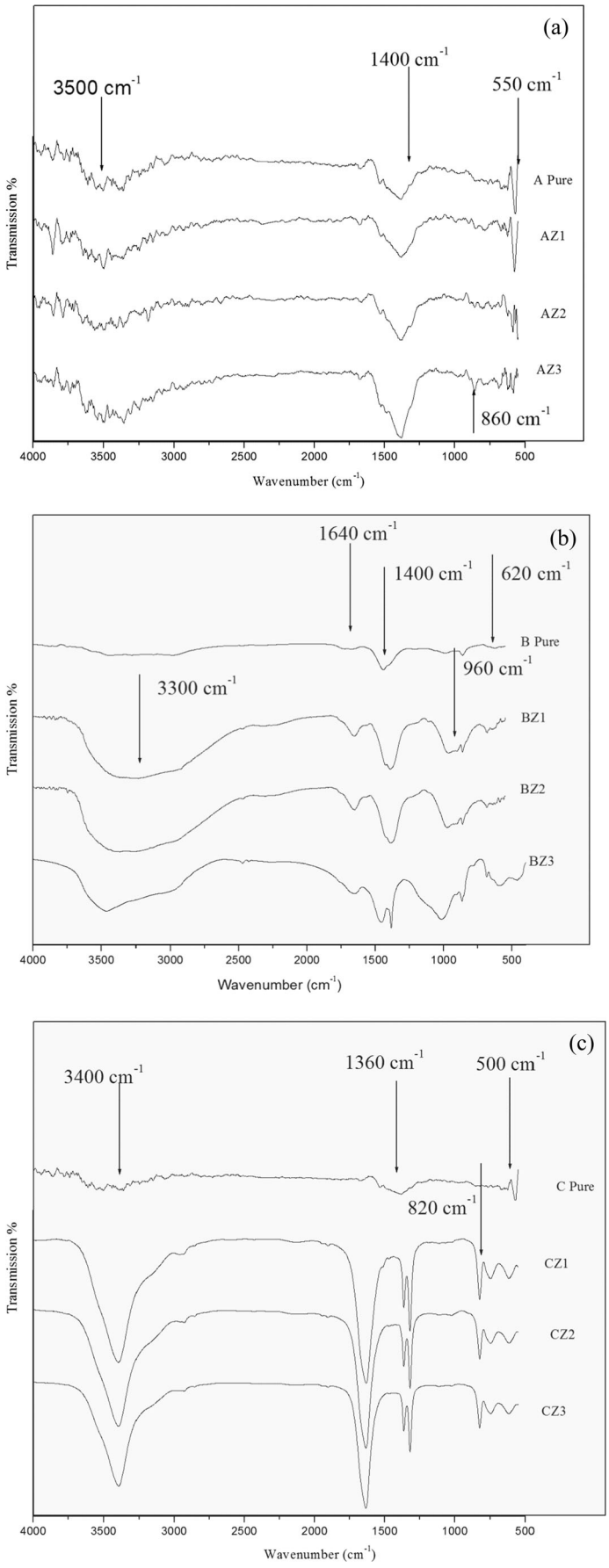

Fig. 4 FTIR spectra of pure and zinc doped yttrium oxide samples prepared by **a** sol–gel, **b** solvothermal and **c** wet chemical methods

Table 3 FTIR analysis details

Vibrational bands of samples (cm^{-1})											Assignments
A Pure	AZ1	AZ2	AZ3	B Pure	BZ1	BZ2	BZ3	C Pure	CZ1	CZ2	CZ3	
3439 1632	3503 1669	3430 1514	3430 1513	3463 1650	3215 1650	3438 1642	3838, 3420 1676	3439 1632	3393 1634	3393 1634	3392 1635	Caused by O-H stretching of the absorbed water reabsorption during the storage of the sample in ambient air
1442	1382	1384	1386	1455, 1383	1390	1392	1442	1442	1364, 1320	1364, 1320	1364, 1320	due to residual nitrate and organic matter in Y_2O_3
	624	847	856		960	1024	861, 989		823, 745	823, 745	827, 746	ZnO stretching
716	567	619	549	684, 599	684	614	623	716, 495	495	495	496	Stretching Frequency of Y–O molecule

FTIR spectra observed of zinc oxide nanoparticles in their investigation. The band around 1300 cm^{-1} is attributed due to residual nitrate and organic matter in Y_2O_3. The results are tabulated in Table 3.

Impedance analysis

Impedance spectroscopy is a simple and powerful tool to study the electrical and dielectric properties of a compacted

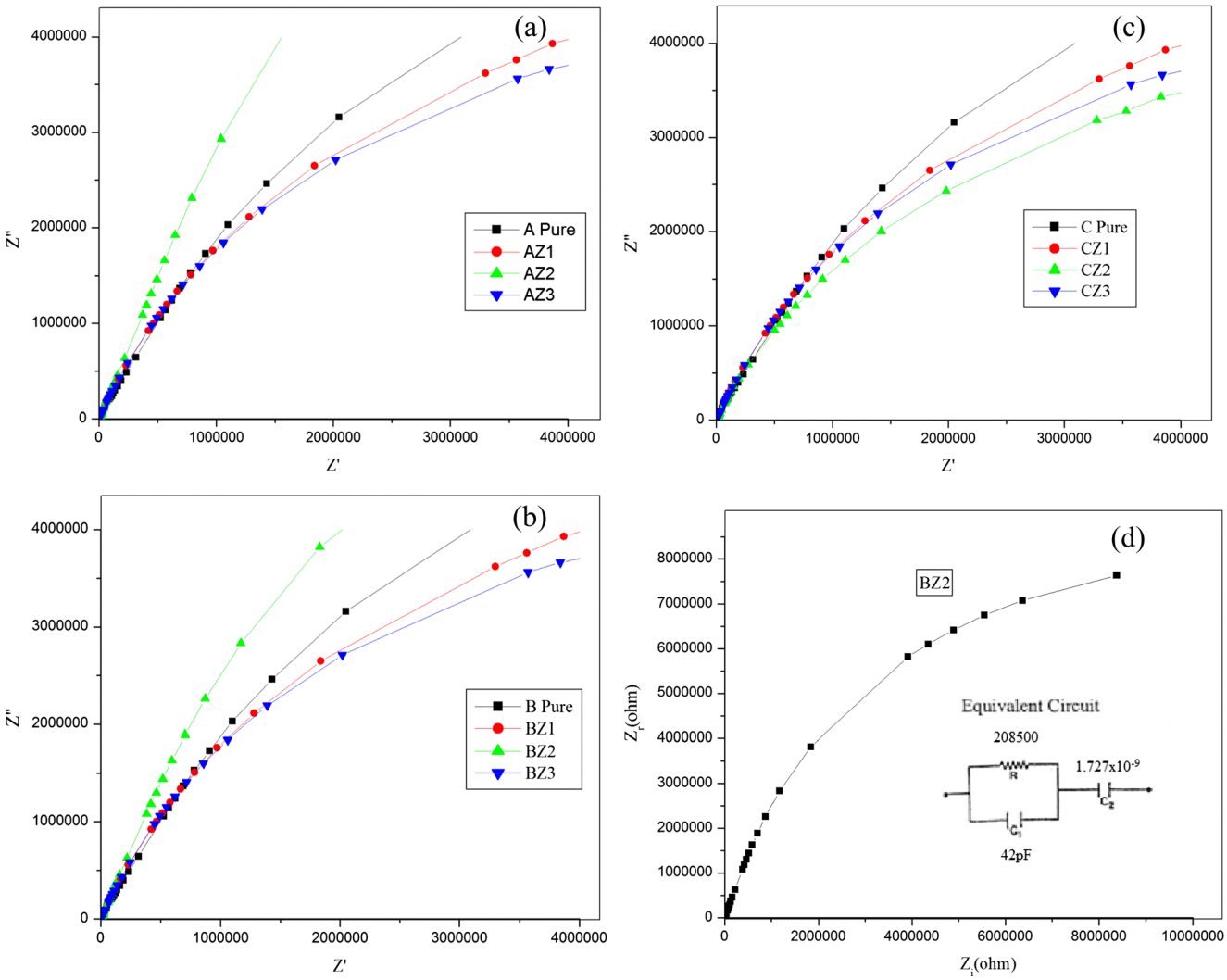

Fig. 5 The complex impedance plots of pure and zinc-doped yttrium oxide samples prepared by **a** sol–gel, **b** solvothermal, **c** wet chemical method at room temperature and **d** complex impedance plot of BZ2 sample along with its equivalent circuit with values

insulating, ionically conducting and semi-conducting materials and their interfaces. Figure 5 shows the complex impedance plots of pure and zinc-doped yttrium oxide samples prepared by sol–gel, solvothermal and wet chemical method at room temperature. It is obvious that all the samples show single semicircular behavior, which suggests the grain resistance in these samples. The low frequency intercepts of the semicircle on the real axis yields bulk resistance (R_b) and is extracted from the impedance plots using EQ software developed by Boukamp [35, 36] and is given in Table 4. It is observed that the diameter of the semicircle increases with the increase in dopant concentration referring to prominent decrease in electrical conduction. At higher frequency region, the semicircle is attributed to the grain property of the materials, which may be due to the parallel combination of resistance and capacitance of the materials. However, the electrical response of material can broadly depend on the structure, composition, particle size and impurities [37–39]. The highest conductivity of the sample BZ2 is due to its amorphous nature. Figure 5d shows the complex impedance plot of BZ2 sample, which has high conductivity along with its equivalent circuit with values in the inset.

The ionic conductivity of the zinc-doped yttrium oxide samples has been evaluated by using the relation

$$\sigma = l/\mathrm{R_bA}$$

where l is the thickness of the pellet and A is its contact area, and the values are tabulated in Table 4. The maximum ionic conductivity of 5.04×10^{-7} $\mathrm{Scm^{-1}}$ has been obtained for the pellet with 50 weight percentage of zinc-doped yttrium oxide prepared by solvothermal method. This may be due to the increase in ionic conductivity and due to the increase in dopant concentration. However, there is slight drop in the conductivity with further increase in dopant concentration. The decrease of conductivity with increase in dopant concentration may be attributed to the fact that the dopants introduce the defect ions in Y_2O_3 system. These defects tend to aggregate due to the diffusion process resulting from sintering and cooling processes. Thus, the increase in dopant concentration increases the defect ions, which facilitates the formation of defect barrier leading to the blockage of flow of charge carriers. This in turn decreases the conductivity of the system [40].

It is clear that conductivity is strongly frequency dependent. The conductivity increases with increasing frequency according to the relation

$$\sigma(\omega)\alpha\omega^{\mathrm{n}}$$

where ω is the angular frequency and the value of n depends on the temperature and frequency. The value of n is found to be in between 0.73 and 0.79 (Table 4). Such a power law dependence on frequency is usually associated with the hopping conduction of electrons. This dependence of conductivity on frequency can be explained by the predominance of the hopping mechanism, as the conductivity increases with increasing frequency [41].

The hopping mechanism in Y_2O_3 nanomaterials is attributed to the presence of oxygen vacancies [42]. Based on the Y_2O_3 bulk electronic structure, the valence band is formed by the filled O-2p orbital and the conduction band is formed by the metal (Y) 5d orbital. The vacancy level forms below the conduction band, and it can also trap one or two electrons. A trapped electron causes the adjacent Y ions to distort asymmetrically, pulling down a singly degenerate B1 state from the conduction band. This state can be occupied by 1 or 2 electrons. The observed dispersion in the resistivity is due to the contribution from the Y and O ions to the relaxation. At low frequency regime, hopping of electrons between the localized

Table 4 The low frequency intercepts of the semicircle on the real axis yields bulk resistance (R_b) and is extracted from the impedance plots using EQ software

Sample name	Conductivity ($\mathrm{Scm^{-1}}$)	Bulk resistance (ohm)	Relaxation time (s)	n	Constant phase element Cz
A Pure	3.5×10^{-7}	210,400	5.35×10^{-5}	0.78	5.47×10^{-10}
AZ1	3.03×10^{-8}	1,842,030	5.77×10^{-7}	0.79	2.68×10^{-10}
AZ2	5.06×10^{-8}	1,455,300	5.33×10^{-7}	0.76	1.21×10^{-9}
AZ3	2.00×10^{-7}	278,189	4.28×10^{-6}	0.77	9.05×10^{-10}
B Pure	3.43×10^{-7}	178,443	5.04×10^{-5}	0.79	6.70×10^{-10}
BZ1	8.93×10^{-8}	668,982	5.23×10^{-6}	0.77	9.90×10^{-10}
BZ2	5.04×10^{-7}	208,500	7.96×10^{-7}	0.73	1.73×10^{-9}
BZ3	5.00×10^{-7}	181,366	7.07×10^{-7}	0.74	2.72×10^{-9}
C Pure	3.52×10^{-7}	182,300	5.36×10^{-5}	0.79	6.13×10^{-10}
CZ1	9.33×10^{-8}	394,720	1.59×10^{-6}	0.77	1.11×10^{-9}
CZ2	2.72×10^{-7}	199,140	1.57×10^{-6}	0.76	1.06×10^{-9}
CZ3	2.79×10^{-7}	174,760	1.59×10^{-6}	0.79	7.60×10^{-10}

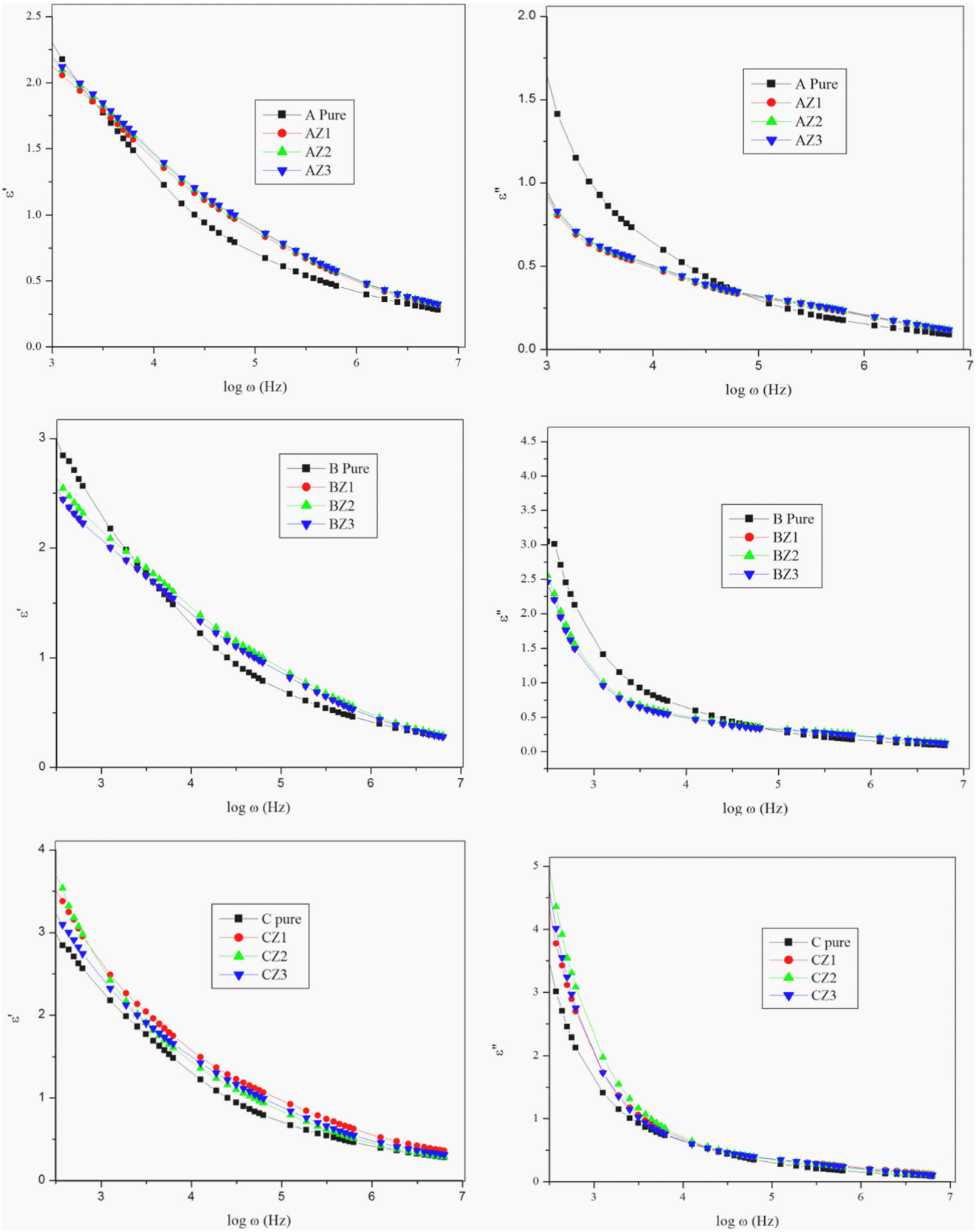

Fig. 6 Variation of dielectric constant and loss factor of pure and zinc-doped Y_2O_3 at room temperature

Y ions increases subsequently the resistivity decreases. At high frequencies, the hopping of electrons could not follow the applied field and hence becomes almost constant (Fig. 6).

Knowing the dielectric constant (ε') of a material is needed to properly design and apply instruments such as level controls using radar, RF admittance, or capacitance technologies. Figure 6 shows the variation of dielectric constant of pure and zinc-doped Y_2O_3 measured as a function of frequency at room temperature, which describes the dissipated energy. It is clear that it has strong frequency dependence in the lower frequency region. It is clearly observed that the dielectric constant decreases with the increase in frequency and becomes almost constant at high frequencies. The higher value of dielectric constant can also be explained on the basis of interfacial/space charge polarization due to inhomogeneous dielectric structure. The polarization decreases with the increase in frequency and then reaches a constant value due to the fact that beyond a certain frequency of external field the hopping between different metal ions (Y^{3+}, Zn^{2+}) cannot follow the alternating field. It has also been observed that the value of dielectric constant decreases with the increase in zinc dopant concentration. The dielectric polarizability of Zn^{2+} (1.7–2.5) is very low compared to yttrium ions (11–15); it might be a reason for the decrease of dielectric constant with the increase in dopant [43]. Hence, as the dopant concentration increases, more yttrium ions will be substituted by zinc ions and thereby decreasing the dielectric polarization, which in turn decreases the dielectric constant.

Dielectric loss can be defined as the amount of power applied to a dielectric in the form of heat energy under the action of voltage. If the electric polarization in a dielectric is unable to follow the varying electric field, dielectric losses occur.

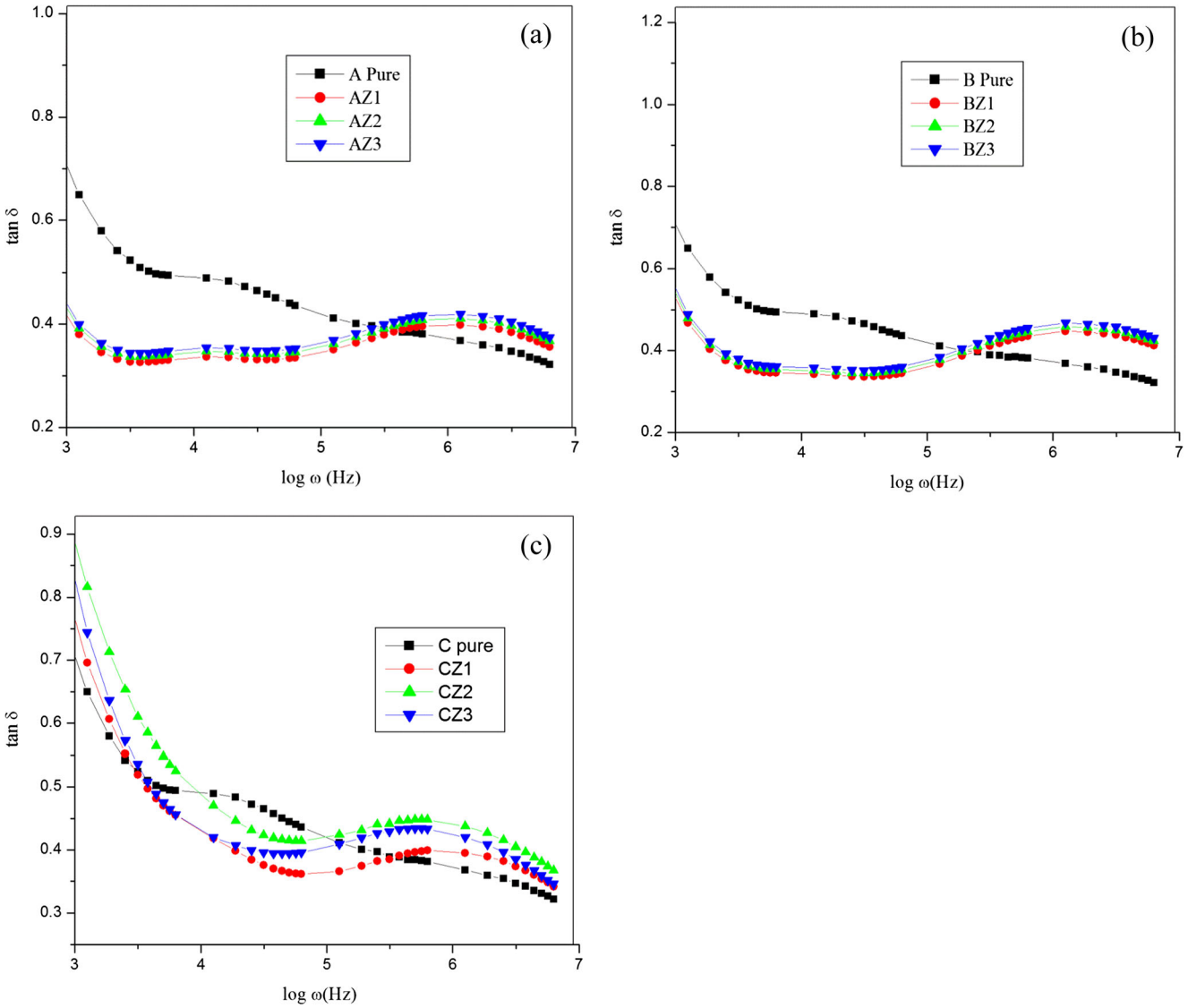

Fig. 7 Variation of dielectric loss factor with frequency at room temperature. **a**) Sol-gel method **b**) Solvothermal method and **c**) Wet chemical method

The measure of ratio of the dielectric loss factor ε'' to the dielectric constant ε' is defined as loss tangent. It is given as

$$\tan\delta = \varepsilon''/\varepsilon'$$

It is useful to obtain relaxation parameters of the samples. Figure 7 shows the variation in dielectric loss factor with frequency at room temperature for zinc-doped yttrium oxide samples prepared by sol–gel, solvothermal and wet chemical methods. From the plots, it is clear that after certain frequency range, tan δ increases with frequency and reaches a maximum value and thereafter decreases. From the loss tangent peak, the relaxation time τ can be estimated using the relation $\omega\tau=1$ and are shown in the Table 4. It indicates low relaxation time 7.96×10^{-7}s for BZ2, leading to the highest ionic conductivity. It is consistent with the conductivity analysis.

It has been observed that dielectric loss decreases with the increase in frequency for all the compositions, which may be due to the space charge polarization. It can also be seen that dielectric loss decreases with the increase in dopant concentration and become very low value at high frequency region, which shows the capability of these materials to be used in high frequency device applications [40].

Conclusion

All zinc-doped yttrium oxide samples show nanocrystalline nature except the one prepared by solvothermal method, with 50 weight percentage of the zinc dopant. The composition of the samples is confirmed by FTIR studies. AC conduction measurement shows the semiconductor properties corresponding to the hopping conduction mechanism. The dielectric constant decreases with increasing frequency. The decrease in dielectric constant is due to the decrease in space charge carries or interfacial polarization in the zinc-doped Y_2O_3 samples. The increase of the dielectric constant with decrease in frequency can be attributed to the presence of dipoles. Dielectric loss decreases with the increase in frequency for all the compositions, which may be due to the space charge polarization. Surprisingly, it was observed that the 50 weight percentage of zinc-doped yttrium oxide samples prepared by solvothermal method, which is amorphous, has more conductivity when compared with other samples.

References

1. Abraham F, Debreuille-Gresse MF, Mairesse G, Nowogrocki G (1988) Phase transitions and ionic conductivity in $Bi_4V_2O_{11}$ an oxide with a layered structure. Solid State Ionics 28–30:529–532
2. Lim DG, Lee JH, Yi JS (2002) Structural and electrical properties of a Y2O3 buffer layer by the two step process. J Korean Phys Soc 40: 167–171
3. Siegel RW (1991) Cluster-assembled nanophase materials. Annu Rev Mater Sci 21:559–578
4. Kodama RH (1999) Magnetic nanoparticles. J Magn Magn Mater 200:359–372
5. Pei Z, Xu H, Zhang Y (2009) Preparation of Cr_2O_3 nanoparticles via C_2H_5OH hydrothermal reduction. J Alloy Compd 468:L5–L8
6. Nickel NH, Jackson WB, Walker J (1998) Influence of grain boundaries on hydrogen transport in polycrystalline silicon J. Non-Cryst Solid 885:227–230
7. Cho Y-J, Shin J-H, Lee J-K, Kim Y-B, Choi D-K (2008) Electrical properties of room temperature sputtered Y2O3 and MOSFET characteristics, In: 7th WSEAS International Conference on Electronics, Hardware, Wireless and Optical Communications, Cambridge, UK, February 20–22
8. Unal O, Akinc M (1996) J Am Ceram Soc 78:805–8
9. Wu Y-M, Lo J-T (1998) Dielectric properties of $PbTiO_3$ thin films on CeO_2/Si(100) and Y_2O_3/Si(100). Jpn J Appl Phys 37:5645. doi: 10.1143/JJAP.37.5645
10. Andreeva AF, Sisonyuk AG, Himich EG (1994) Growth conditions, optical and dielectric properties of yttrium oxide thin films. Phys Stat Sol A 145:441–446
11. Manning WR, Hunter O Jr, Powell BR Jr (1969) Elastic properties of polycrystalline yttrium oxide, dysprosium oxide, holmium oxide and erbium oxide: Room temperature measurements. J Am Ceram Soc 52:436–437
12. Single oxides: Y (1981) Engineering property data on selected ceramics, vol 3, Single oxides, Metal and Ceramics Information Center, Battelle memorial institute, Columbus, OH.
13. Ling CH, Bhaskaran J, Choi WKAH,LK (1999) Study of RF-sputtered yttrium oxide films on silicon by capacitance measurements. J Appl Phys 77:6350–3
14. Cho M-H, Ko D-H, Jeong K, Whangbo SW, Whang CN (1999) Structure transition of crystalline Y2O3 film grown on Si(111) with substrate temperature. Thin Solid Films 349:266
15. Kwo J, Hong M, Kortan AR, Queeney KT, Chabal YJ, Mannaerts JP, Boone T, Krajewski JJ, Sergent AM, Rosamilla JM (2000) High k- gate dielectrics of Gd_2O_3 and Y_2O_3 for silicon. Appl Phys Lett 77:130–132
16. Ramana CV, Mudavakkat VH, Kamala BK, Atuchin VV, Pokrovsky LD, Kruchinin VN (2011) Enhanced optical constants of nanocrystalline yttrium oxide thin films. Appl Phys Lett 98: 031905
17. Zhao Y, Kita K, Kyuno K, Toriumi A (2009) Band gap enhancement and electrical properties of La_2O_3 films doped with Y_2O_3 as high k-gate insulators. Appl Phys Lett 94: 042901
18. Cho JY, Ko K-Y, Do YR (2007) Optical properties of sol–gel derived $Y_2O_3:Eu^{3+}$ thin-film phosphors for display applications. Thin Solid Films 515:3373–3379
19. Rastogi AC, Sharma RN (1992) Structural and electrical characteristics of metal-insulator-semiconductor diodes based on Y_2O_3 dielectric thin films on silicon. J Appl Phys 71:5041. doi:10.1063/1.350605
20. Hammad TM, Salem JK, Harrison RG (2009) Synthesis characterization, and optical properties of Y-doped ZnO nanoparticles. Nano 04:225. doi:10.1142/S1793292009001691
21. Bhavani G, Ganesan S (2012) Synthesis of nano ytrrium oxide phosphors by simple methods and their morphological studies. Int J Phys 1(1):32–40
22. Hristea A, Popovici EJ, Muresan L, Grecu R, Indrea E, Voicescu M (2004) Yttrium tantalate based phosphors for X-ray intensifying screen, Romopto 2003. Seventh Conference on Optics 5581:781–787. Published: 2004

23. Muresan L, Popovici EJ, Hristea A, Vasilescu M, Silaghi-Dumitrescu I (2004) Studies on the synthesis of terbium activated gadolinium oxysulphide phosphors, Romopto 2003: Seventh Conference on Optics 5581:775–780. Published: 2004
24. Popovicia E-J, Muresan L, Amaliaa H, Indrea E, Vasilescuc M (2007) Synthesis and characterisation of europium activated yttrium oxide fine powders. J Alloys Compd 434–435:809–812
25. Muresan L, Popovicia E-J, Grecua R, Tudoran LB (2009) Studies on the synthesis of europium activated yttrium oxide by wet-chemical method: 1. Influence of precursor quality on phosphor photoluminescence properties. J Alloys Compd 471(1–2):421–427
26. Muresan L, Popovici E-J, Indrea E (2011) Structural and luminescence characterization of yttrium oxide based phosphors prepared by wet- chemical method. J Optoelectron Adv Mater 13(3): 183–189
27. Korzenski MB, Lecoeur P, Mercey B, Camy P, Doualan JL (2001) Low propagation losses of an Eu:Y2O3 planar waveguide grown by alternate target pulsed laser deposition. App Phys Lett 78:1210–1212
28. Zhang S, Xiao R (1998) Yttrium oxide films prepared by pulsed laser deposition. J App Phys 83:3842–3848
29. Evangelou EK, Wiemer C, Fanciulli M, Sethu M, Cranton W (2003) Electrical and structural characteristics of yttrium oxide films deposited by rf magnetron sputtering on n-Si. J App Phys 94:318–325
30. HosseiniVajargah S, Madaah Hosseini HR, Nemati ZA (2006) Synthesis of nanocrystalline yttrium iron garnets by sol–gel combustion process. The influence of pH of precursor solution. Mater Sci Eng B 129:211–215
31. Xiaoyi S, Yuchun Z (2011) Preparation and optical properties of Y_2O_3/SiO_2 powder. Rare Met 30:33–38
32. Rao CNR (1963) Chemical applications of infrared spectroscopy. Academic Press, New York
33. Markova-Deneva I (2010) Infrared spectroscopy investigation of metallic nanoparticles based on copper, cobalt, and nickel synthesized through borohydride reduction method. J Univ Chem Technol Metall 45:351–378
34. Parthasarathi V, Thilagavathi G (2011) Synthesis and characterization zinc oxide nano particles and its application on fabrics for microbe resistant defense clothing. Int J Pharm Pharm Sci 3(4): 392–398
35. Boukamp BA (1986) A nonlinear least squares fit procedure for analysis of immittance data of electrochemical systems. Solid State Ionics 20:31–44
36. Boukamp BA (1986) A package for impedance/admittance data analysis. Solid State Ionics 18&19:136–140
37. Markovic S, Miljkovic M, Jovallekic C, Mentus S, Uskokovic D (2009) Densification, microstructure and electrical properties of BaTiO3 (BT) Ceramics prepared from ultrasonically De-Agglomerated BT powders. Mater Manufac Proces 24(10–11): 1114–1123
38. Irvine JTS, Sinclair DC, West AR (1990) Electroceramics: characterization by impedance spectroscopy. Adv Mater 2:3,132–138
39. Byeon SC, Hong KS, Park JG, Kang WN (1997) Origin of the increase in resistivity of manganese–zinc ferrite polycrystals with oxygen partial pressure". J Appl Phys 81(12):7835–7841
40. Azam A, Ahmed AS, Chaman M, Naqvi AH (2010) Investigation of electrical properties of Mn doped tin dioxide nanoparticles using impedance spectroscopy. J Appl Phy 108(9):094329-094329-7
41. Kudo K, Sumimotu T, Hiraga K, Kuniyoshi S, Tanaka K (1997) Evaluation of electrical properties of evaporated thin films of metal free copper and PbPc by In-Situ field effect measurements. J Appl Phys Jpn 36:6994–6998
42. Ikeda S, Ogawa K (1992) Structure Images of Y_2O_3 corresponding to the shift of Y-atoms. J Electron Microsc 41:330–336
43. Shannon RD (1993) Dielectric polarizabilities of ions in oxides and fluorides. J Appl Phy 73(1):348–366